1967-05

The effects of sensible heat exchange on the dynamics of baroclinic waves

Haltiner, G.J.

Wiley Online

Haltiner, G. J. "The effects of sensible heat exchange on the dynamics of baroclinic waves." Tellus 19.2 (1967): 183-198.
http://hdl.handle.net/10945/60196

The effects of sensible heat exchange on the dynamics of baroclinic waves

By G. J. HALTINER, *U.S. Naval Postgraduate School, Monterey, California*

(Manuscript received December 1, 1965)

ABSTRACT

A diabatic two-level model with variable static stability is investigated with respect to the dynamic stability and thermal structure of harmonic perturbations. The exchange of sensible heat is assumed to be proportional to the difference in temperature between the air and the underlying surface. This type of diabatic heating reduces the instability of short and medium waves and shifts the maximum instability to a shorter wave length than the corresponding adiabatic model; however, the instability of long waves is increased. Solution of the initial value problem for various initial phase differences between the stream function wave, thermal wave and static stability waves show the importance of these parameters with respect to the growth characteristics which are complex. Limiting angles for a 4000-km wave length show an 85° lag of the thermal wave behind the stream wave and the latter lagging the vertical velocity and static stability waves by about 90° and 110° degrees respectively; but no significant differences are found between the adiabatic and diabatic cases. For an 8000-km wave length, the thermal wave lags the stream wave by about 30° and the stream wave, in turn, lags the static stability and vertical velocity waves by 140° with adiabatic flow, while with heat exchange the corresponding figures are 25° and 105°.

Introduction

The increase in speed and storage capacity of electronic computers attained during the past decade has made possible the integration of complex numerical prediction models on an operational basis. As a result meteorologists have been able to add more physics to the models by way of consistent energetics, terrain conditions, friction, heat sources, as well as finer grids, larger areas and improved finite differencing. Despite numerous attempts during this period to develop a simple baroclinic model which will correctly predict the development of pressure systems, the results have not lived up to expectations. In fact, a one parameter model is still quite widely used for mid-tropospheric prediction. Recently BENGTSSON (1964) carried out a series of experiments with several "two-level" models including various combinations of terms in the vorticity and thermodynamic equations, some of which were inconsistent with respect to vorticity and/or energy conservation. He noted that these physical inconsistencies in certain models gave rise to significant errors. For example, the ordinary two-level quasi-geostrophic model tends to overpredict kinetic energy. Bengtsson concluded that a fundamental error in the two-level models is the tendency for the thermal wave to approach a limiting phase lag behind the pressure wave which then leads to continued amplification. This conclusion was based in part on the results of his experiments and in part on the results of OGURA (1957), THOMPSON (1959), and WIINNIELSEN (1960), who showed that for an adiabatic, frictionless, quasi-geostrophic, two-level model with constant static stability, an unstable wave will amplify when the thermal wave lags the pressure wave and damping occurs when thermal wave precedes the pressure wave. Ogura and Wiin-Nielsen further showed for linearized models that regardless of the initial lag, the phase difference between the thermal wave and the unstable pressure wave tends toward a limiting value with the former lagging the latter, thus eventu-

ally giving rise to amplification. Bengtsson's non-linear model yielded similar results but gave a somewhat larger phase lag than predicted by linear theory.

In the actual atmosphere the thermal wave tends to lag during the developing stage of the wave cyclone but catches up during the mature stage with the atmosphere finally becoming quasi-barotropic.

HALTINER & CAVERLY (1965) considered a quasi-geostrophic, two-level model with surface friction based on an Ekman layer. They found that the friction not only reduces the amplification of synoptic waves, but in addition showed that the phase difference between an unstable pressure wave and its thermal wave decreased with increasing surface drag coefficient, thus more nearly approximating conditions in nature than the frictionless case.

In view of these results it also appears desirable to determine the effects of diabatic heating on the dynamic stability and thermal structure of baroclinic waves, including the phase relationship between the pressure and temperature waves. DÖÖS (1964) studied the influence of sensible heat exchange on planetary flow by means of a linearized, quasi-geostrophic model with constant static stability and obtained stationary analytic solutions for a particular, but realistic, zonal wind profile. The exchange of sensible heat was assumed to be proportional to the temperature difference between the underlying surface and the air, and also a decreasing function of pressure. The temperature of the underlying surface was a prescribed periodic function while the air temperature depended on the motion. DÖÖS considered only long wave lengths in consonance with the ocean-continent arrangement at 45° latitude which gives two maxima and minima in the observed east-west temperature distribution. He found the center of the heat source to be about 30° to the west of the temperature maximum of the underlying surface. With respect to the wind field, the heat source for the air was located near the maximum equatorward surface wind components; and the heat sink, near the poleward surface winds.

The present investigation considers the influence of sensible heat transfer on the dynamic stability and other properties of harmonic perturbations superimposed on a zonal current. Since the heat transfer affects the temperature distribution and hence the static stability and these parameters, in turn, influence the properties of the perturbations, it was considered desirable to utilize a model which permits variations in static stability.

LORENZ (1960) designed a "two-layer" model with a variable, self-determining static stability which also possesses consistent integral properties with respect to vorticity and energy. GATES (1961) has studied this model in considerable detail and showed that in the adiabatic, frictionless case, greater baroclinic instability is found in wave lengths of 2000 to 5000 km with a variable static stability than in the conventional two-parameter quasi-geostrophic 1953 model of Charney and Phillips (see also BENGTSSON, 1964).

Mathematical development

The basic equations are the vorticity equation, thermodynamic equation, continuity equation and the linear portion of the balance equation, namely

$$\nabla^2\Phi - \nabla\cdot(f\nabla\psi) = 0.$$

The atmosphere is separated into four 250-mb layers by five pressure levels denoted by 0, 1, 2, 3, and 4, in order of increasing pressure. The sum and the difference of the vorticity equations at levels 1 and 3 are formed and a similar procedure is followed with respect to the thermal equation. Finally, the balance equation is differentiated with respect to p to give a type of thermal wind equation. The procedure is similar to that of GATES (1961), except for the addition of the heating terms in the thermal equations.

The results are

$$\frac{\partial\nabla^2\psi}{\partial t} + J(\psi, \nabla^2\psi + f) + J(\tau, \nabla^2\tau) = 0, \quad (1)$$

$$\frac{\partial\nabla^2\tau}{\partial t} + J(\tau, \nabla^2\psi + f) + J(\psi, \nabla^2\tau) - \nabla\cdot(f\nabla\chi) = 0, \quad (2)$$

$$\frac{\partial\theta}{\partial t} + J(\psi, \theta) + J(\tau, \sigma) - \nabla\cdot(\sigma\nabla\chi) = \frac{Q_1 + Q_3}{2}, \quad (3)$$

$$\frac{\partial\sigma}{\partial t} + J(\tau, \theta) + J(\psi, \sigma) - \nabla\theta\cdot\nabla\chi = \frac{Q_1 - Q_3}{2}, \quad (4)$$

$$2^{-(1+\varkappa)}R\nabla^2\theta - \nabla\cdot(f\nabla\tau) = 0. \quad (5)$$

Here

$$\psi = (\psi_1 + \psi_3)/2, \quad \tau = (\psi_1 - \psi_3)/2,$$

$$\theta = (\theta_1 + \theta_3)/2, \quad \sigma = (\theta_1 - \theta_3)/2,$$

$$\chi = (\chi_3 - \chi_1)/2 \quad \text{and} \quad \varkappa = R/c_p,$$

where ψ is the stream function; θ, the potential temperature; and χ, the velocity potential for the divergent wind. Q_1 and Q_3 are heating rates at levels 1 and 3, respectively. No friction has been included and the vertical velocity ω has been assumed to be zero at levels, 0 and 4. The continuity equation gives

$$2\omega = p_4 \nabla^2 \chi,$$

where ω is the vertical motion at level 2.

The equations are to be linearized assuming a basic zonal current with vertical shear but no horizontal shear. It will be further assumed that in the basic state no diabatic heating is occurring and the surface air is in thermal equilibrium with the underlying surface. The latter must therefore have a lateral temperature gradient consistent with the thermal wind relationship.

Heating

The exchange of sensible heat at the surface is taken to be proportional to the temperature difference between the air and the underlying surface. Further, the heating is assumed to be a decreasing power of pressure similar to Döös (1962) as follows:

$$Q = A V_s (T_g - T_s) \left(\frac{p}{p_s}\right)^r.$$

Here A and r are constants, V_s and T_s are the surface wind and air temperature and T_g is the temperature of the underlying surface. Since the equations are to be linearized by assuming a small perturbation superimposed on a basic flow, the variation of the surface wind speed above will be neglected leading to

$$Q = K(T_g - T_s) \left(\frac{p}{p_s}\right)^r, \tag{6}$$

where K is a constant.

The earth's surface is assumed to be an infinite heat source or sink so that its temperature field remains constant while the air temperature tends to adapt to that of the surface. As shown by Döös (1962) and others, this condition is more nearly approached over the ocean than land; however, no distinction is made in this study.

Since the surface air temperature has been assumed to be in thermal equilibrium with the underlying surface in the undisturbed state, only the perturbation temperatures really need be considered. The simplest approach is to merely extrapolate from the 750-mb level to obtain the temperature at 1000 mb, in which case the air-sea temperature difference is simply $(\theta - 2\sigma)$, if we take the lower boundary to be at 1000 mb. The heating functions then become

$$\begin{aligned} Q_1 &= K(2\sigma - \theta)\,(\tfrac{1}{4})^r, \\ Q_3 &= K(2\sigma - \theta)\,(\tfrac{3}{4})^r, \end{aligned} \tag{7a}$$

where σ and θ are to be regarded as perturbation quantities.

A more accurate estimate may be obtained by taking into account the deviation of the sea-level pressure from 1000 mb. With some minor approximations the additional term for the sea-level air temperature perturbation may be written

$$\left[\Gamma_d - \left(\frac{\partial\theta}{\partial p}\frac{\partial p}{\partial z}\right)_0\right] \frac{f}{g}(\psi - 2\tau). \tag{7b}$$

Here ψ and τ again represent perturbation quantities, whereas the other parameters are from the basic state; and Γ_d is the dry adiabatic lapse rate. Multiplication by $-K(p/p_0)^r$ yields the heating terms to be added to (7a). Substitution of typical values into (7a) and (7b) show the latter to be essentially an order of magnitude less than the former.

Linearization of the system (1) through (5), together with the assumption of harmonic solutions of the form $\psi \exp ik(x - ct)$, $\tau \exp ik(x - ct)$, $\Theta \exp ik(x - ct)$, $S \exp ik(x - ct)$, and $X \exp ik(x - ct)$, leads to a system of homogeneous linear equations

$$MN = 0, \tag{8}$$

where M is the matrix

$$\begin{vmatrix} c-U+\beta/k^2 & -U^* & 0 & 0 & 0 \\ -U^* & c-U+\beta/k^2 & 0 & 0 & -if/k \\ \dfrac{-2^{\varkappa+1}fU^*}{R}-q_1 vi & \dfrac{2^{\varkappa}(1-\varkappa)fU^*}{R}+\dfrac{2q_1 vi}{k} & -\left(c-U+\dfrac{iq_1}{k}\right) & U^*+\dfrac{2iq_1}{k} & -ik\sigma_0 \\ \dfrac{2^{\varkappa}(1-\varkappa)fU^*}{R}+\dfrac{q_2 vi}{k} & \dfrac{-2^{\varkappa+1}fU^*}{R}-\dfrac{2q_2 vi}{k} & U^*+\dfrac{iq_2}{k} & -\left(c-U+\dfrac{2iq_2}{k}\right) & 0 \\ 0 & -f & R2^{-(1+\varkappa)} & 0 & 0 \end{vmatrix} \tag{9}$$

and N is a column vector made up of the coefficients ψ, τ, Θ, S, X.

A necessary and sufficient condition that the system (8) has a non-trivial solution is that the determinant of the coefficients vanish. The resulting frequency equation is cubic with respect to the phase velocity c and yields the dynamic stability characteristics of the current at a function of wave length, thermal wind, latitude, heating function, etc. By eliminating the difference in the stream functions τ and the potential function for the divergent wind component χ, the system may be reduced to

$$a_{11}E + a_{12}\Theta = 0, \tag{10}$$

$$a_{21}E + a_{22}\Theta + a_{23}\sigma = 0, \tag{11}$$

$$a_{31}E + a_{32}\Theta + a_{33}\sigma = 0, \tag{12}$$

where $E = g\psi/f$, $q_1 = \dfrac{K}{c_p}\dfrac{3^r+1}{2^{2r+1}}$,

$$q_2 = \frac{K}{c_p}\frac{3^r-1}{2^{2r+1}},$$

$$\left.\begin{aligned} a_{11} &= c-U+\beta/k^2, \quad a_{12} = -U^*R/f2^{(1+\alpha)}, \\ a_{21} &= -\frac{2^{(\varkappa+1)}fU^*}{R}+\frac{k^2U^*\sigma_0}{f}, \\ a_{22} &= \frac{(1-\varkappa)U^*}{2}-\left(c-U+\frac{iq_1}{k}\right) \\ &\quad -\frac{k^2\sigma_0 R(c-U+\beta/k^2)}{f^2 2^{(1+\varkappa)}}, \\ a_{23} &= U^*+\frac{2iq_1}{k}, \quad a_{31} = \frac{2^{\varkappa}(1-\varkappa)fU^*}{R}, \\ a_{32} &= \frac{iq_2}{k}, \quad a_{33} = -\left(c-U+\frac{2iq_2}{k}\right). \end{aligned}\right\} \tag{13}$$

Corresponding to each of the roots c_j of the frequency equation there is an "eigenvector" (E_j, Θ_j, S_j). The Θ_j and S_j may be obtained from two of the three equations above, e.g. (10) and (11), in terms of E_j, which is to be considered arbitrary for the present. In view of the latter condition, the general solution to the linearized differential system may be expressed in the form

$$\left.\begin{aligned} E &= \sum_{j=1}^{3} E_j \exp ik(x-c_j t), \\ \theta &= \sum_{j=1}^{3} \Theta_j \exp ik(x-c_j t), \\ \sigma &= \sum_{j=1}^{3} S_j \exp ik(x-c_j t). \end{aligned}\right\} \tag{14}$$

In order to study the evolution of some particular disturbances, the following initial conditions will be specified

$$\left.\begin{aligned} E(t=0) &= A \exp ikx, \\ \theta(t=0) &= A_T \exp i(kx+\alpha), \\ \sigma(t=0) &= A_S \exp i(kx+\delta). \end{aligned}\right\} \tag{15}$$

From (14) and (15) it follows immediately that

$$\left.\begin{aligned} \sum_{j=1}^{3} E_j &= A, \\ \sum_{j=1}^{3} \Theta_j &= A_T \exp i\alpha, \\ \sum_{j=1}^{3} S_j &= A_S \exp i\delta. \end{aligned}\right\} \tag{16}$$

The three equations above, plus the six equations resulting from the use of (10) and (11) with each value of c_j, $j = 1, 2, 3$, permit the determination of the E_j, Θ_j, and S_j in terms of the initial amplitudes of the stream function, thermal wave and static stability waves, A, A_T and A_S, respectively, the phase lags α and δ, and the other parameters such as L, U^*, f, β, σ_0, q_1, q_2, etc.

Though each of the quantities E, Θ and S has three wave components according to (14), each may be written as a single wave with an amplitude and phase angle which are functions of time. Let the phase velocity be expressed as the complex number

$$c_j = c_{jr} + ic_{ji}. \tag{17}$$

Then from (14)

$$E = \sum_{j=1}^{3} (E_{jr} + iE_{ji})\, e^{kc_{ji}t} e^{-ikc_{jr}t} e^{ikx}$$

$$= \sum_{j=1}^{3} E_{jM} e^{i\varepsilon_j} e^{ikx}, \tag{18}$$

where

$$E_{jM} = e^{kc_{ji}t}(E_{jr}^2 + E_{ji}^2)^{\frac{1}{2}}, \tag{19}$$

$$\varepsilon_j = \arctan \frac{E_{ji}}{E_{jr}} - kc_{jr}t. \tag{20}$$

Next, the amplitude E_M and phase angle E_p of the wave solution E, which are functions of time as well as other parameters, may be expressed as

$$E_M = [(\sum_{j=1}^{3} E_{jM} \cos \varepsilon_j)^2 + (\sum_{j=1}^{3} E_{jm} \cos \varepsilon_j)^2]^{\frac{1}{2}}, \tag{21}$$

$$E_p = \arctan \frac{\sum_{j=1}^{3} E_{jM} \sin \varepsilon_j}{\sum_{j=1}^{3} E_{jM} \cos \varepsilon_j} \tag{22}$$

In a similar fashion the potential temperature perturbation may be expressed in terms of a magnitude and phase angle which will be denoted by the symbols θ_M and θ_p, respectively; the static stability magnitude by σ_M and its phase angle by σ_p; and the vertical velocity magnitude by ω_M and its phase angle by ω_p.

Numerical results

A. Dynamic stability

The dynamic stability characteristics of the model were first determined by setting the determinant of the matrix (9) to zero and finding the roots of the frequency equation for a variety of values of wave length, thermal wind and heating functions. Since the effect of latitude variations on the stability of baroclinic waves is well known the latitude was fixed at 45° in all cases. Figures 1*a*, 1*b*, 1*c* and 1*d* show the three values of c in m/s, both the real and imaginary parts, as functions of wave length for thermal winds of 0, 5, 10 and 15 m/s under adiabatic conditions. The barotropic case ($U^* = 0$) gives three real roots, as is well known. The diagrams show the familiar increase in instability with increasing thermal wind and are included only for comparison to the diabatic cases. Over the band of unstable wave lengths there is one neutral, one amplified, and one damped wave, the latter two having the same propagation rates. The two dashed curves are diabatic examples which will be discussed presently.

Figures 2*a*, 2*b*, 2*c* and 2*d* are similar to Figure 1 except that heating is included. The heating constants for this case have been chosen as follows:

$$K = 100 \text{ ergs g}^{-1} \text{ °K}^{-1} \text{ sec}^{-1}, \; r = 2,$$

which is similar to values used by Döös (1962) in his study of stationary perturbations. Then for each 1°C of temperature difference between the air and surface, there is a heat transfer of 100 ergs g^{-1} sec^{-1}. For $r = 2$, this corresponds to a total heat transfer of 63 cal per square centimer per day in the entire column of air for each degree of temperature difference.

The choice of r determines the rate at which the heating decreases with height. Observations indicate that the major part of the heating takes place in the lower ten thousand feet but extends in significant amounts up to 500 mb.

In these first examples, the correction to the sea-air temperature difference for the deviation of the surface perturbation pressure from 1000 mb (7b) was omitted. The barotropic case, $U^* = 0$, gave two essentially neutral waves and one damped wave. The diagrams in Figure 2, when compared to the adiabatic examples in Figure 1, show that this form of diabatic heating tends to reduce the growth rates in the intermediate wave lengths but extends the region of amplified waves to longer wave lengths. Bearing in mind that the actual growth rate is proportional to c_i/L, and not just c_i, it may be seen that the heat exchange also tends to shift the wave length of maximum growth rate toward a shorter wave length, by about 1000 km for the cases shown. The cutoff of instability at short wave lengths, however, is quite similar

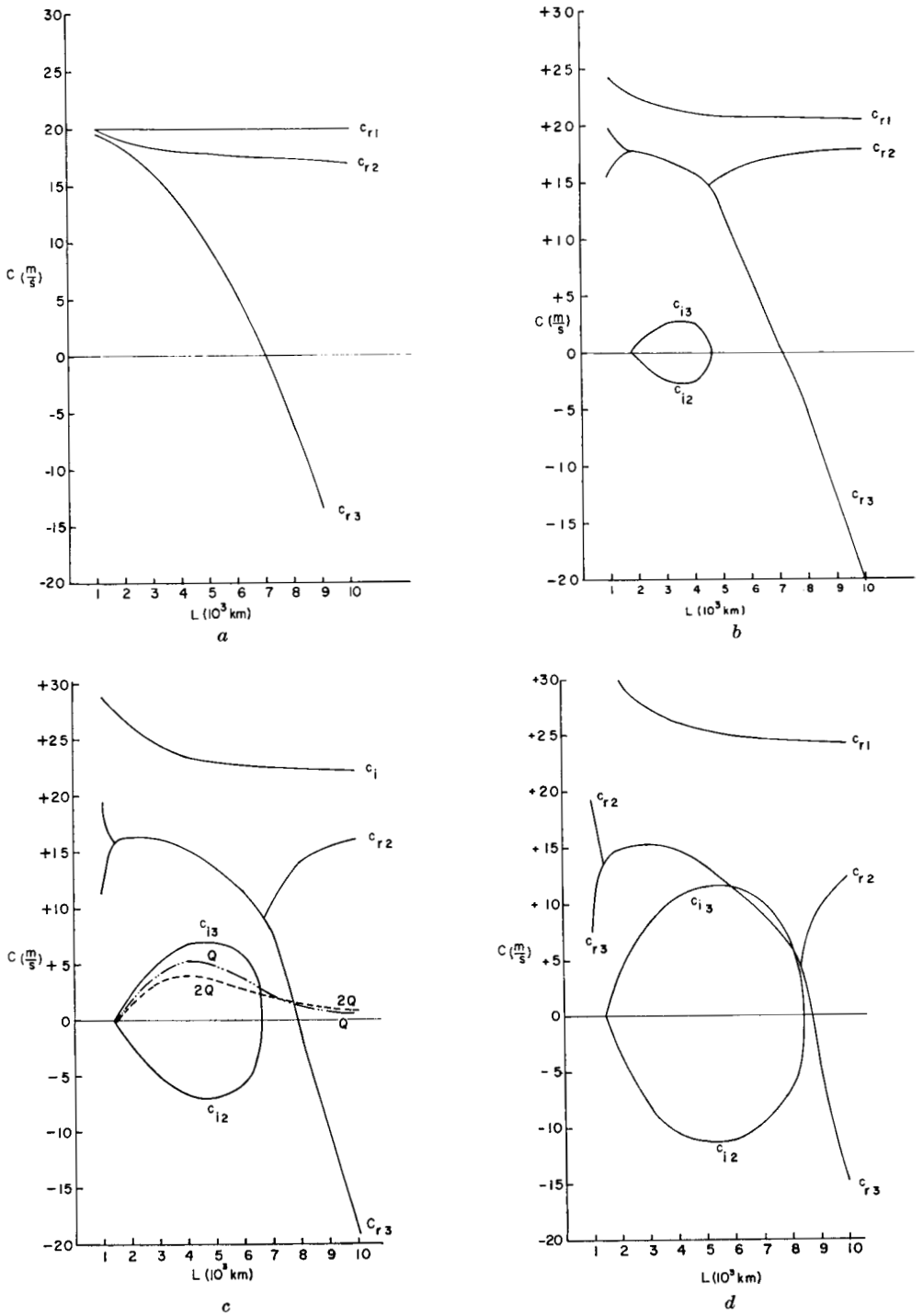

Fig. 1. Phase velocities (ordinate) in meters per second for the adiabatic case for thermal wind values of (*a*) 0, (*b*) 5 m/s, (*c*) 10 m/s, and (*d*) 15 m/s as a function of wave length (abscissa) in units of 10^3 km. c_r is the real part and c_i, the imaginary part. The dashed curve in 1*c* gives c_i for the diabatic case of Figure 2*c*. The dash-dot curve labeled 2*Q* corresponds to a doubling of the heating rate.

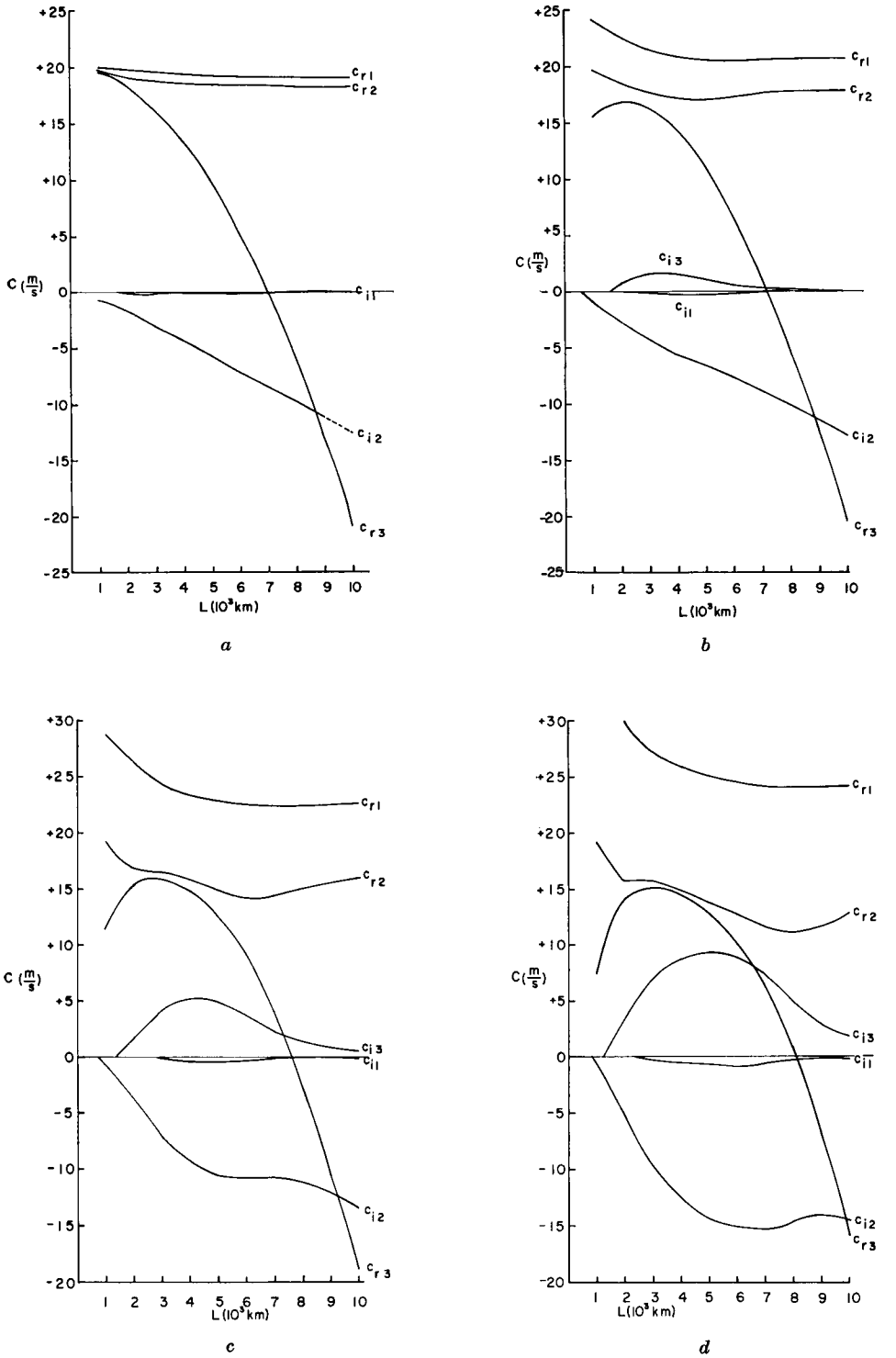

Fig. 2. Diabatic case similar to Figure 1.

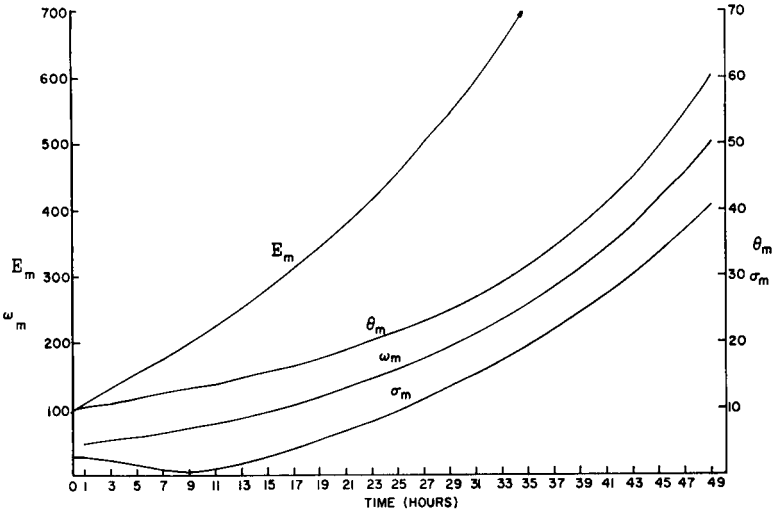

Fig. 3a. Amplitudes (ordinate), E_M (meters), θ_M (degrees), σ_M (degrees) and ω_M (10^{-4} mb sec^{-1}), of the stream, potential temperature ,static stability and vertical velocity waves as functions of time (abscissa) for $L = 4000$ km, $U^* = 15$ m/s, $\alpha = 90°$, $\delta = 90°$, $K = 100$ ergs g^{-1} $°C^{-1}$ sec^{-1}, $r = 2$.

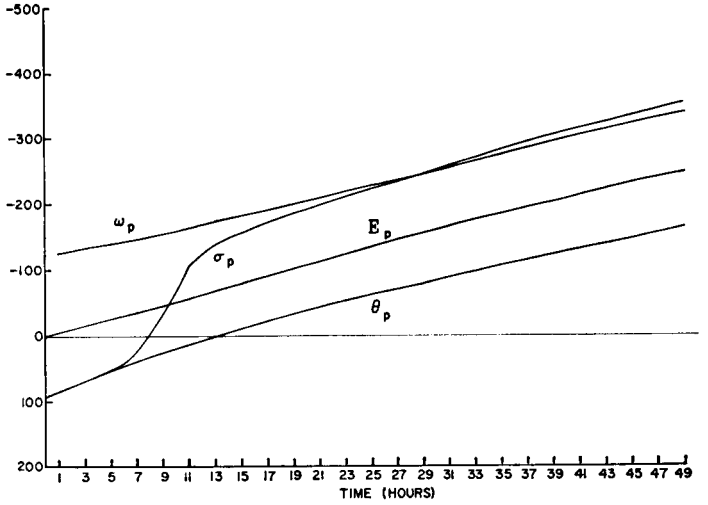

Fig. 3b. Phase angles (ordinate, in degrees) E_p, θ_p, σ_p, and ω_p as functions of time (abscissa) in hours for the case shown in Figure 3*a*.

in the adiabatic and diabatic cases. For easier comparison, the curve of c_i for the amplified waves with heating and a thermal wind of 10 m/s is included in Figure 1*c*, labeled as *Q*. The curve labeled 2*Q* in Figure 1c corresponds to a doubling of the heating rate per degree of temperature difference between the surface and the air. Here a further reduction in the amplification rate may be noted for the intermediate wave lengths, however at wave lengths over 7000 km the instability has been increased slightly with the greater rate of heat exchange. This is consistent with the increased instability at long wave lengths when heating occurs.

Some other features of the cases with heating are noteworthy. For all thermal wind values, there is one wave with only very slight damping, thus being essentially neutral. Its propagation rate which is roughly 25 m/s corresponds closely to the neutral wave in the adiabatic

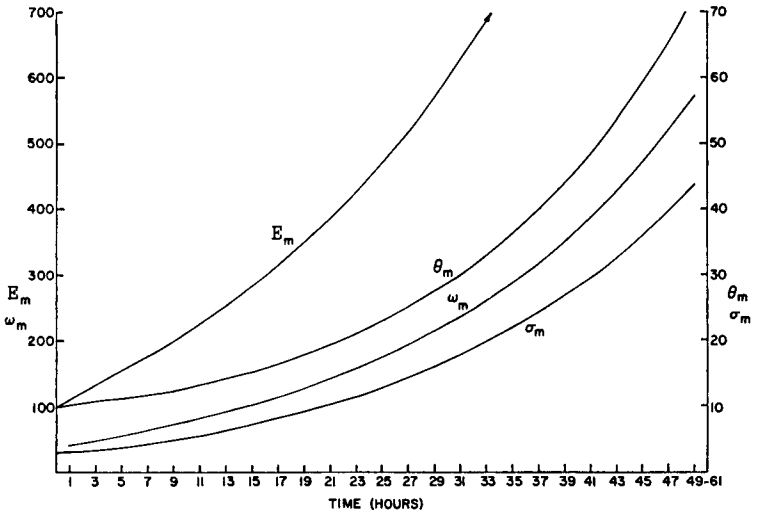

a

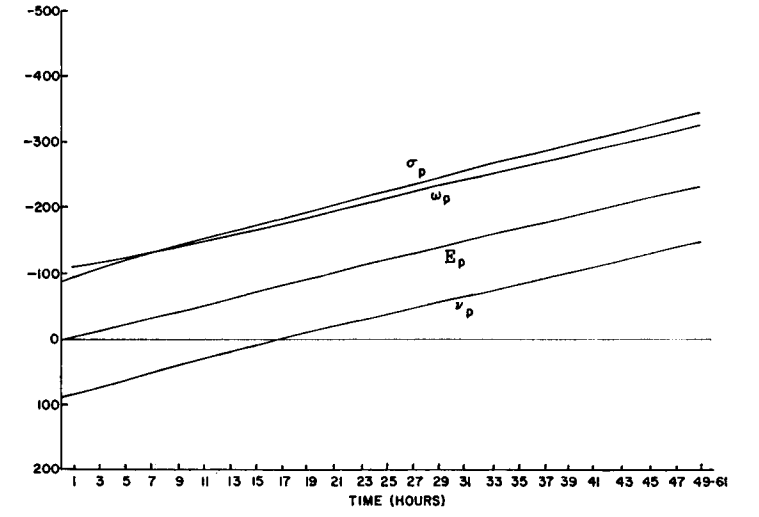

b

Fig. 4. Similar to Figure 3 except that $\delta = -90°$.

case. The damped wave in each diabatic case corresponds somewhat to the damped adiabatic wave; however the damping is much stronger at long wave lengths and has a slightly different point of cutoff on the short side. Here again the propagation rates of the waves with and without heating differ somewhat, especially near the cutoff of instability on the long wave side with adiabatic flow.

Finally, it should be observed that the eastward propagation rates of the amplified waves correspond closely to those of Rossby-type and show the characteristic retrogression of the long waves. The waves move somewhat slower when heating is present than under adiabatic conditions, differences of five knots are common with the stronger thermal winds.

The essential differences between the diabatic and adiabatic cases are brought out adequately in the diagrams shown, though many other computations were made. For example, when the vertical distribution of heating was changed

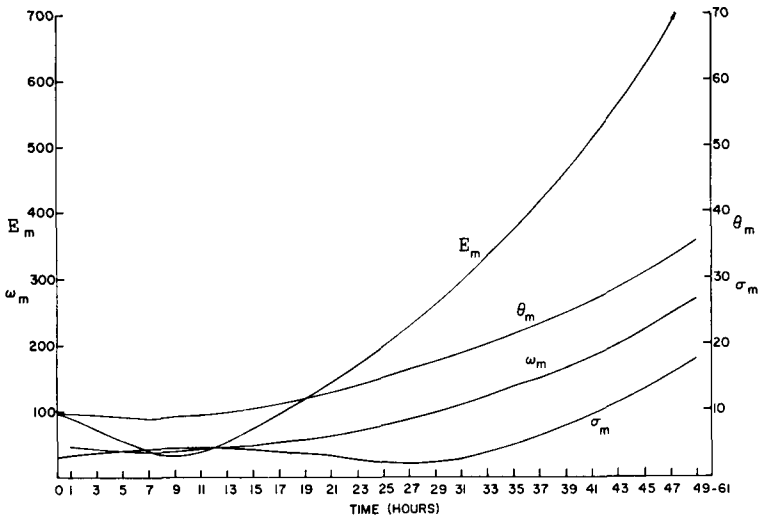

a

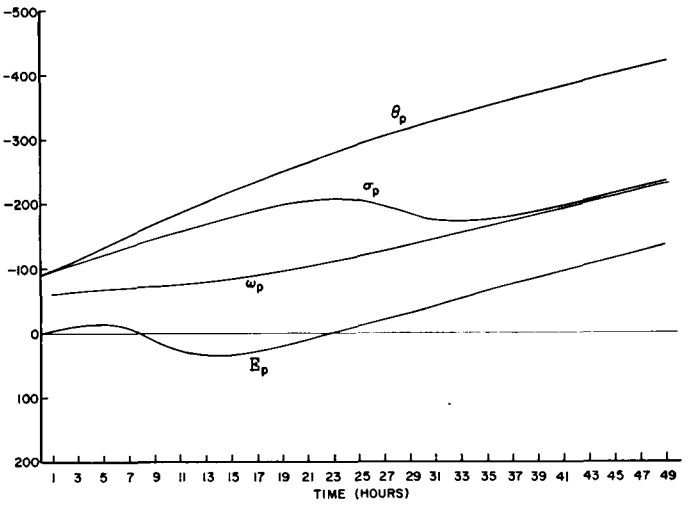

b

Fig. 5. Similar to Figure 3 except that $\alpha = \delta = -90°$.

to a linear function of pressure, the results differed only slightly from the quadratic case. Similarly, a series of computations which included the corrections to the surface temperatures stemming from the perturbations in the sea-level pressure field (see Eq. 7b) differed negligibly from those utilizing only the heating functions 7a.

B. Initial value problem

Calculations were next carried out to determine the amplitudes and phase angles of the stream function, potential temperature, static stability and vertical velocity waves as functions of time for varying initial conditions as well as for various values of other pertinent parameters governing the flow. The computations were extended to 61 hours in each case, which is beyond the period reasonably valid for the linearized problem, in order to ascertain, if possible, limiting phase angles between the stream function, potential temperature, static stability and vertical velocity waves. Graphical displays of some typical examples will be shown;

however these cases represent only a small fraction of the many for which calculations were completed. In all of the cases shown certain parameters were held constant as follows:

$$U = 20 \text{ m sec}^{-1};\ U^* = 15 \text{ m sec}^{-1};\ f = 45°;$$

$$K = 100 \text{ ergs g}^{-1}, {}^{\circ}C^{-1} \text{ sec}^{-1} \text{ or } K = 0;\ r = 2;$$

$$A = 100 \text{ m};\ A_T = 10°\text{C};\ A_S = 3°\text{C or } 0.$$

The first set of cases to be discussed, which are shown in Figures 3, 4, and 5, are for a wave length of 4000 km. While this wave length is not the most unstable wave, it certainly is typical in behavior.

(*a*) $L = 4000$ km

Figure 3*a* shows the amplitudes E_M, θ_M, σ_M and ω_M as functions of time (abscissa) for initial phase lags of $\alpha = 90°$ and $\delta = 90°$ for the thermal and static stability waves, respectively. Diabatic heating is included. Except for an initial decrease in the amplitude of the static stability wave, all waves grow rapidly in amplitude. Figure 3*a* shows the corresponding phase angles E_p, σ_p and ω_p in degrees (ordinate). Here a slope upward to the right represents a progression eastward and a downward slope, retrogression. Also when the curve of a particular parameter lies below that of another, the former lags the latter. Note that the phase relationship between the pressure and thermal waves remains essentially constant, whereas the static stability wave moves rapidly eastward as it decreases in amplitude and catches up to the stream function wave in about 9 hours. By 15 hours the static stability wave is well ahead of the stream wave, after which it forges slowly ahead. The vertical velocity wave, which is computed from a diagnostic equation, is found initially to be about 120° ahead of the stream wave but gradually decreases to about 90° where it remains, implying downward velocities between the ridge and the downwind trough.

The adiabatic case corresponding to Figure 3 is qualitatively similar to the diabatic case except that the growth of all waves is greater. Table 1 gives the amplitudes for this case and others at 31 hours and also the phase differences in degrees between the stream wave and each of the other waves at 61 hours. A negative phase difference indicates that the stream wave precedes the other wave, whereas a positive value indicates a lag of the stream wave.

Figure 4 is similar to 3 except that $\delta = -90°$. All waves grow slightly more rapidly in this case. Also the static stability wave does not show the initial decrease in amplitude found in the first case, nor does the phase relationship between the static stability wave and stream wave change significantly with time. In this example the vertical velocity and static stability waves are essentially in phase at the onset and amplification of the latter begins immediately. This also evidently favors somewhat greater growth of the stream wave, about 5 % more than the first case.

Figure 5 represents the case when the thermal wave initially precedes the stream wave, i.e., $\alpha = -90°$; also $\delta = -90°$. As expected, the stream wave begins to decrease in amplitude, and the thermal wave also decreases slightly. On the other hand, the thermal wave progresses steadily eastward while the stream wave moves only slightly forward and then retrogresses until about 14 hours. At the time of minimum amplitude of the stream wave, namely, 9 hours, the stream and thermal waves are 180° out of phase. Thereafter the thermal wave assumes a lagging position with respect to the stream wave and the latter begins to amplify. The static stability wave progresses eastward for the 20 hours, then remains stationary for about 5 hours, retrogresses for another 6 to 8 hours, and finally becomes essentially in phase with the ω-wave beyond about 36 hours some 100 degrees or so ahead of the stream wave. The perturbation static stability reaches its minimum amplitude of 2°C during its period of retrogression.

The adiabatic case corresponding to Figure 5 behaved in a qualitatively similar fashion; only the magnitudes were different as shown in Table 1.

Computations were carried out for many other initial values of α and δ. When the two waves are initially in phase, the stream wave moves steadily ahead of the thermal wave giving rise to amplification immediately; however the growth rate is less than in the first case discussed (Figure 3). The amplitude of the thermal wave is almost constant for about 35 hours, and then gradually increases; whereas the amplitude of the static stability wave increases from the beginning.

TABLE 1. *Amplitudes E_M (meters), θ_M (°C), σ_M (°C), $\omega(10^{-4}$ mb sec$^{-1})$ at 31 hours and phase differences $(E_p-\theta_p)$, $(E_p-\sigma_p)$, and $(E_p-\omega_p)$ in degrees at 61 hours for $L=4000$ km and for various α and δ (degrees) and heating conditions.*

$A=100$ meters, $A_T=10$°C, $A_S=3$°C or $A_S=0$ when δ denoted with an asterisk.

Heating	α	δ	E_M	θ_M	σ_M	ω_M	$E_p-\theta_p$	$E_p-\sigma_p$	$E_p-\omega_p$
0	90	180	801	45.4	26.9	327	−84	117	94
0	90	−90	757	43.3	29.0	318	−84	118	94
0	180	−90	752	45.6	24.2	314	−84	115	93
0	180	180	677	38.9	19.6	273	−84	115	94
0	90	90	671	34.9	22.5	265	−85	117	94
0	180	0	642	38.2	23.4	272	−84	117	94
0	90	0	618	32.2	25.0	255	−85	118	94
0	180	90	552	29.8	18.6	223	−85	117	94
0	0	180	462	25.5	18.5	190	−85	117	94
0	0	90	446	23.8	14.5	170	−86	116	93
0	−90	0	351	24.2	8.5	143	−83	113	94
0	0	−90	325	15.7	16.8	137	−85	121	95
0	−90	−90	315	21.3	5.2	125	−92	112	93
0	0	0	302	12.7	12.2	107	−88	118	93
Q	90	180	686	33.2	16.2	250	−85	112	92
Q	180	−90	644	34.3	14.4	242	−84	111	92
Q	90	−90	625	30.0	17.7	235	−85	113	93
Q	180	180	609	31.0	12.5	222	−84	111	92
Q	90	0*	606	27.8	16.4	221	−85	114	93
Q	90	90	597	26.7	15.0	211	−86	113	86
Q	180	0*	570	28.8	13.3	212	−84	112	93
Q	180	90	498	28.8	13.3	212	−84	112	93
Q	0	0*	309	12.1	10.0	105	−88	116	92
Q	−90	−90	295	18.5	2.7	108	−81	105	92
Q	0	0	268	9.8	8.8	82	−92	115	91
Q	−90	0*	232	14.3	2.6	84	−82	106	92
Q	−90	180	184	10.8	1.2	65	−83	104	91
Q	−90	90	184	11.3	3.1	67	−83	107	92
$2Q$	90	180	607	25.8	11.0	204	−84	106	91
$2Q$	90	90	546	21.6	10.5	178	−86	107	91
$2Q$	90	−90	537	22.0	11.4	185	−85	108	92
$2Q$	0	0	246	8.7	6.8	68	−94	110	89

When the thermal and stream waves are 180° out of phase initially, the latter is stationary for the 8 hours or so while the former moves steadily eastward so that a favorable condition for growth is present immediately, similar to in-phase case. The vertical velocity wave remains about 90° ahead of the stream wave the entire period, whereas the static stability wave is nearly stationary for about one day when it becomes nearly in phase with the vertical velocity wave. The phase relationships between the various waves change little after 24 hours.

Table 1 summarizes results for the wave lengths of 4000 km. The examples are tabulated in order of decreasing amplitude of the stream function but separately for the adiabatic and the diabatic cases (denoted by Q and $2Q$), the latter showing significantly smaller amplitudes. Note that initial phase of the static stability wave plays an important role with respect to amplification as well as that of the thermal wave. It should be recalled here that the mean static stability, σ_0, is the same for all cases. By and large, θ_M and ω_M decrease with decreasing E_M, but σ_M shows a few significant reversals. The 8th, 9th and 10th columns give the phase differences between the E-wave and each of the θ, σ, ω-waves. Here a negative value implies a lag of one of latter three with respect to the E-wave. The average lag of the thermal wave is 85°, while the vertical velocity wave precedes the E-wave by an average of 92°. There is no difference between the adiabatic and diabatic

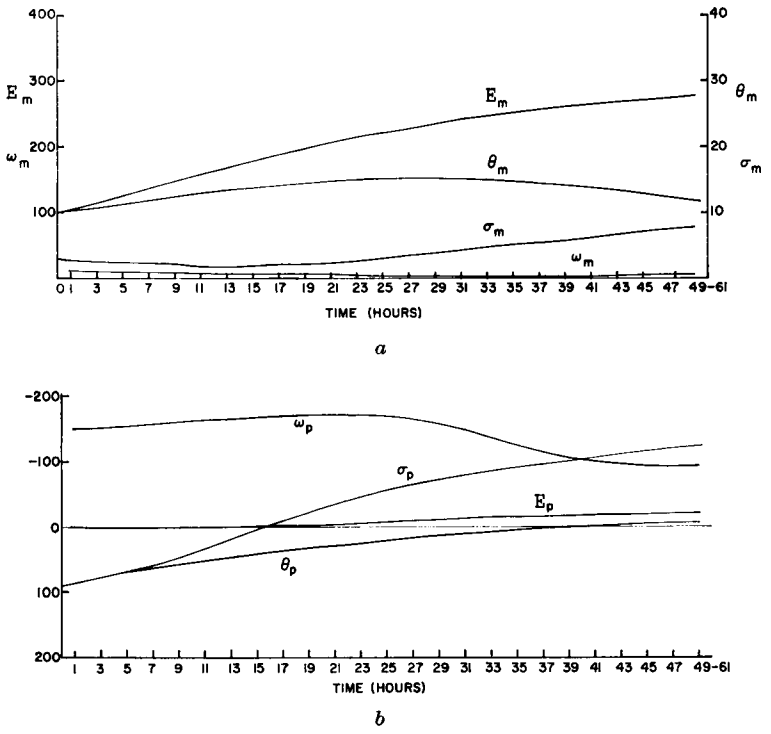

Fig. 6. Similar to Figure 3 except that $L = 8000$ km, $\alpha = \delta = 90°$.

cases here. On the other hand, the static stability wave precedes the stream wave by an average of 116° in the adiabatic case and 108° in the diabatic case, a rather small difference.

(*b*) $L = 8000$ km

Next, some results are presented for a wave length of 8000 km which has some characteristic differences from the 4000 km length. As shown in the Figure 2, the dynamic instability is much less than for the 4000 km wave.

Figure 6 shows the diabatic case with $\alpha = \delta = 90°$. Amplification begins immediately as expected, but the rate decreases with time contrary to the case, $L = 4000$ km, where the rate of amplification steadily increased during the period of integration. The thermal wave amplifies at first and then decreases in amplitude after about 28 hours, whereas the static stability wave is damped slightly for about one-half day and then amplifies during the remainder of the period. The vertical velocities are much smaller than for the 4000-km wave. The final phase difference between the stream and thermal waves again shows a lag of the latter, but only about 25°. The static stability and vertical velocity waves again precede the stream wave, by about 120° and 80° respectively. With regard to other propagation characteristics shown in Figure 6*b*, the stream wave is seen to be very slightly progressive, averaging less than five knots. The thermal wave progresses eastward at about 40 knots during the first 20 hours eventually slowing to about the same speed as the stream wave. The adiabatic case corresponding to Figure 6 is qualitatively similar, but differences in magnitudes occur as illustrated in Table 2.

Computations for the diabatic case $\alpha = \delta = -90°$ show damping and marked retrogression in the early stages but in about 11 hours the thermal wave is in a lagging position and amplification begins. By 27 hours retrogression had ceased and slight progression follows. Both the thermal and static stability waves progress rapidly eastward; however the former first decreases in amplitude and then increases,

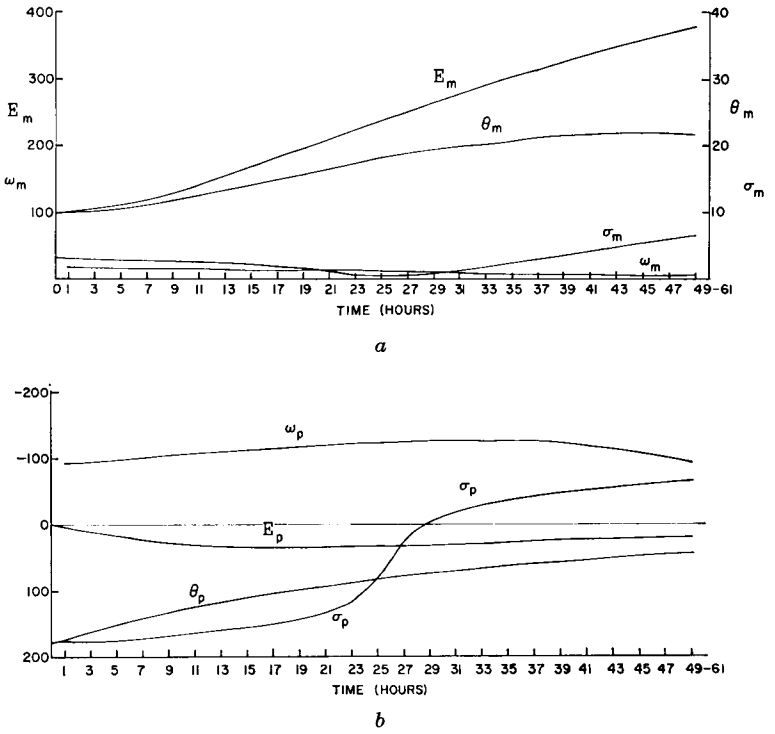

Fig. 7. Similar to Figure 6 except that $\alpha = \delta = 180°$.

while the latter increases slightly and then decreases to about 1° by about 41 hours. The final phase differences between the waves are quite similar to the preceding case.

Of the diabatic examples computed, the warm trough–cold ridge combination ($\alpha = 180$) showed the greatest amplification for the wave length of 8000 km as shown in Figure 7 and Table 2. Here the initial retrogression of the stream wave and the progression of the thermal wave gives rise immediately to a lagging thermal wave favorable for amplification which persists throughout the period. The thermal wave also amplifies the maximum, reaching a peak at about 45 hours.

Table 2 summarizes the calculations for the 8000 km wave. The 61-hour period was not quite adequate to establish truly limiting phase differences, however the results are consistent except for the damped cases. Again the adiabatic examples generally showed greater amplification, but only by about 10 % here. The average lag of the thermal wave is about 30° for the adiabatic case and 25° for the diabatic examples. On the other hand, the static stability and vertical velocity waves precede the stream wave by about 140° under adiabatic conditions and only about 105° when heating is included, a substantial difference.

Calculations were also made for wave lengths of 2000, 6000 and 10,000 km. The shortest of these waves showed a periodic character to the amplitude and phase but also marked growth. The behavior of the 6000 km wave was more or less midway between the 4000 and 8000-km waves which have been discussed in detail. The period of 61 hours was too short to allow the full character of the long 10,000-km waves to unfold; however it was similar to the 8000-km wave, though with smaller growth and greater retrogression.

Summary and conclusions

The results of this investigation show that the exchange of sensible heat as simulated here tends to reduce the dynamic instability of short and medium length perturbations and also shifts the wave length of maximum instability toward a shorter value than for the correspond-

Table 2. *Similar to Table 1 except that L = 8000 km.*

Heating	α	δ	E_M	θ_M	σ_M	ω_M	E_p–θ_p	E_p–σ_p	E_p–ω_p
0	180	− 90	325	27.9	6.6	18	−31	143	145
0	180	0	301	24.0	8.7	16	−35	150	143
0	90	− 90	300	23.6	8.8	13	−32	153	143
0	180	180	298	24.1	30.4	13	−29	134	133
0	90	180	297	24.5	4.9	11	−29	140	134
0	180	90	272	19.5	6.4	12	−36	143	132
0	90	0	263	17.7	9.1	9	−38	154	135
0	90	90	260	18.9	5.3	7	−27	145	125
0	− 90	− 90	163	15.9	3.0	13	−28	125	155
0	− 90	0	163	17.2	4.7	14	−33	145	157
0	− 90	90	125	11.9	3.8	10	−39	145	146
0	− 90	180	125	10.0	1.1	8	−32	119	128
0	0	180	128	11.0	4.0	2	−25	157	142
0	0	− 90	104	5.6	6.5	4	−39	183	145
0	0	90	97	11.0	1.3	3	3	110	19
0	0	0	71	5.5	5.3	5	−73	200	137
Q	180	− 90	290	21.2	1.7	12	−23	103	101
Q	180	180	280	20.0	1.4	10	−20	103	86
Q	180	0*	269	18.3	2.2	10	−25	110	98
Q	90	180	269	18.3	2.2	6	−20	112	85
Q	90	− 90	258	15.8	4.0	7	−30	123	102
Q	180	90	249	15.6	3.5	8	−30	118	96
Q	90	0*	248	15.1	3.9	9	−30	124	93
Q	90	90	241	15.1	4.4	3	−28	123	83
Q	− 90	− 90	156	14.2	2.5	11	−21	75	122
Q	− 90	0*	134	11.4	1.1	9	−25	87	121
Q	− 90	180	131	10.1	1.1	8	−21	89	100
Q	− 90	90	112	8.8	1.2	8	−32	105	124
Q	0	0*	84	4.8	3.4	4	−85	184	115
Q	0	0	62	5.5	4.9	6	−72	−121	155

ing adiabatic case. However, the instability of the longer "planetary" waves is increased by the diabatic processes. It should be noted that the average gain of heat energy over one wave length is zero by virtue of the periodic character of the heating function.

The numerical solutions to the initial value problem bear out the dynamic instability results by showing a reduction in the amplification of the stream wave when diabatic heating is included. Calculations for the wave length of 4000 km clearly show limiting phase differences between the stream function, temperature, static stability and vertical velocity waves; however the differences between the adiabatic and diabatic cases are slight, at least for the rates of heating assumed here. The thermal wave lags the stream wave as shown in earlier studies while the vertical velocity and static stability waves precede the stream wave. The last result differs somewhat from Bengtsson's calculations with a non-linear model which showed the static stability maximum lagging the stream function, in fact, almost coinciding with the trough.

The 61-hour period of integration was not adequate to give truly limiting phase differences for the 8000-km wave in every case; however the essential characteristics were apparent. Here amplitudes were again reduced but also substantial changes were noted between the final phase differences of the E-wave and the α and ω-waves when the heat exchange was included.

The limiting lag of the thermal wave behind the stream function wave and the concomitant amplification has been described as a fundamental shortcoming of the two-level model. However, in view of the differences in the behavior of short and long waves it might be conjectured that an initial disturbance, often of short wave length as evidenced by synoptic charts, lengthens as the system intensifies. As a result the limiting phase difference between

the pressure and thermal waves would then tend toward a smaller value in three or four days, particularly if friction reduces the lag still more. Thus predictions from a two-level model may not differ radically from observations in this respect.

There is a well known tendency for pressure systems to develop off the east coasts of continents in winter which is generally ascribed to the addition of energy through sensible and latent heat from the warm ocean. Although much more complex, this situation bears a relation to the present investigation. On the basis of the results obtained here it is evident that mere warming of air behind the trough and cooling ahead would not bring about intensification. However if the air ahead of the trough comes off a cold land mass and heat energy is added from the relatively warm ocean, intensification can take place. Some unpublished computations by the author demonstrate that a stationary heat source ahead of the trough will produce intensification.

Acknowledgements

The author wishes to express his thanks to Mr. R. Brunell of the U.S. Naval Postgraduate School Computing Facility for effecting the numerical computations, and to Mrs. Joyce Lindley for typing the manuscript.

REFERENCES

Bengtsson, L., 1964, Some numerical experiments on the effect of the variation of static stability in two-layer quasi geostrophic models. *Tellus*, **16**, 328–348.

Döös, B. R., 1962, The influence of exchange of sensible heat with the earth's surface on the planetary flow. *Tellus*, **14**, 133–147.

Gates, W. L., 1961, The stability properties and energy transformations of the two-layer model of variable static stability. *Tellus*, **13**, 460–471.

Haltiner, G. J., and Caverly, D. E., 1965, The influence of friction on the growth and structure of baroclinic waves. *Quarterly Journal of the Royal Meteorological Society*, **91**, 209–214.

Lorenz, E. N., 1960, Energy and numerical weather prediction. *Tellus*, **12**, 364–373.

Ogura, Y., 1957, Wave solutions of the vorticity equation for the $2\frac{1}{2}$-dimensional model. *Journal of Meteorology*, **14**, 60–64.

Thompson, P. D., 1959, Some statistical aspects of the dynamical processes of growth and occlusion in simple baroclinic models. *The Rossby Memorial Volume*, Stockholm 1959, 350–358.

Wiin-Nielsen, A. C., 1960, A note on the thermal structure of waves in a simple baroclinic model. *Technical Memorandum*, No. 17. Joint Numerical Weather Prediction Unit, National Meteorological Center, Washington, D.C.

ВЛИЯНИЕ ТЕПЛОВОГО ОБМЕНА НА ДИНАМИКУ БАРОКЛИННЫХ ВОЛН

С помощью неадиабатической двухуровенной модели с переменной статической устойчивостью исследуется динамическая устойчивость и термическая структура гармонических возмущений. Обмен теплом принимается пропорциональным разности температур воздуха и подстилающей поверхности. Этот тип неадиабатического нагревания уменьшает неустойчивость коротких и средних волн и сдвигает максимум неустойчивости в сторону коротких волн по сравнению с адиабатической моделью; однако, неустойчивость длинных волн возрастает. Решение задачи с начальными данными для различных начальных разностей фаз волны функции тока, температурной волны и волны статической устойчивости обнаруживает важность этих параметров для характеристик роста возмущений, причем эти характеристики являются комплексными. Предельные углы для 4000-км волны дают 85° для отставания термической волны по отношению к волне функции тока, а последняя отстает от волн вертикальной скорости и статической устойчивости на 90° и 110° соответственно; существенной разницы между адиабатическим и неадиабатическим случаями не обнаружено. Для 8000-км волны, термическая волна отстает от волны функции тока приблизительно на 30°, а волна функции тока, в свою очередь, отстает от волн статической устойчивости и вертикальной скорости на 140° для адиабатического потока, тогда как с учетом теплообмена соответствующие цифры составляют 25° и 105°.